Two-wave-plate compensator method for full-field retardation measurements

Carole C. Montarou, Thomas K. Gaylord, Brent L. Bachim, Alexei I. Dachevski, and Abhiruchi Agarwal

The two-wave-plate compensator (TWC) method is expanded for full-field retardation measurements by use of a polarization microscope. The sample image is projected onto a CCD camera connected to a computer, allowing the retardation to be measured at all pixels. The retardation accuracy of this implementation of the TWC is evaluated to be 0.06 nm. The method is applied to polarization-maintaining fibers and long-period fiber gratings. The measured retardation is in good agreement with the crossed-polarizer images of the fibers. The method achieves a spatial resolution of 0.45 μm and a retardation resolution of 0.07 nm. The full-field TWC method can thus be a useful tool for characterizing and monitoring the fabrication of optical devices.

OCIS codes: 110.0180, 120.4640, 260.1440.

1. Introduction

Birefringence can occur naturally owing to structural symmetry. It can also be induced, in which case measuring the birefringence allows the evaluation of the physical and optical properties of a sample. Consequently, birefringence measurements benefit a plethora of applications. In crystallography, birefringence may be caused by lattice mismatch during crystal growth.[1–3] In fluid dynamics, white-light interference colors are produced by a two-dimensional flow and are related to refractive-index gradients.[4] Birefringence measurements allow the characterization of thin films[5] and the quality control of glass and plastics.[6,7] In biology, the dynamic observation of living cells is made possible by real-time birefringence measurements.[8,9] Birefringence is also related to the structure of the retinal nerve fiber layer in the human eye and can be used for the early detection of glaucoma.[10] In optical communications, stress-induced birefringence affects the quality, reliability, and performance of optical fibers and devices. It renders the transmission response of planar light-wave circuits polarization sensitive, which is an undesirable effect in optical networks.[11–17] In optical fibers, birefringence is induced by residual stress through the stress-optic effect. The residual stress profile is closely related to the refractive-index profile that governs the waveguiding properties of the fiber.[18–21] Birefringence causes polarization-mode dispersion and polarization-dependent loss.[22–25] Stress-induced birefringence plays a crucial role in the refractive-index changes that occur during the fabrication of long-period fiber gratings with CO_2 laser pulses.[26–30]

Several techniques have been developed to evaluate two-dimensional birefringence through optical retardation measurements. In optical fibers and devices, the retardations produced are of the order of several nanometers. Hence the methods used must be able to measure exceedingly small retardations. An instrument that was introduced previously uses photoelastic modulators to modulate the polarization of the light incident upon the birefringent sample.[31–37] Two-dimensional measurements are performed by scanning the sample. The main limitation of this technique is its poor spatial resolution because it uses a single-beam illumination of ~1 mm diameter.

For higher spatial resolution, a microscope system must be used. Oldenbourg and Mei[38] and Schribak and Oldenbourg[39] incorporated electro-optic modulators into a polarization microscope to record several images for various voltage settings.[38,39] This system has been applied to the dynamic observation of living cells.[8,9] The technique relies, however, on intensity measurements, which are not, in general, as accurate

The authors are with the School of Electrical and Computer Engineering, Georgia Institute of Technology, 777 Atlantic Drive NW, Atlanta, Georgia 30332-0250. T. K. Gaylord's e-mail address is tgaylord@ece.gatech.edu.

Received 7 July 2005; revised 23 August 2005; accepted 26 August 2005.

0003-6935/06/020271-10$15.00/0

as detecting a null of intensity. Further, it does not use the simple, conventional compensators that are commonly available with a polarization microscope.

A half-shade device method has been used to profile the residual stress in ultraviolet-exposed optical fibers. The image of the fiber is divided into two parts by the half-shade device. In this technique, one subtracts two intensity profiles on either side of the half-shade boundary along the axis of the fiber image to calculate the retardation and subsequently the residual stress profile to be computed.[40] However, the method does not take into account the axial variations of the fiber in that two intensity lines are subtracted at two different locations along the fiber.

Another technique uses an inverted polarization microscope and the Sénarmont technique to measure the residual stress profile of optical fibers.[30,41–43] The Sénarmont technique is commonly used to measure retardations up to 1λ. However, this technique is not generally suitable for low retardations.

This situation has motivated the development of a high-accuracy technique based on detecting a null of intensity that would be implementable for full-field retardation measurements. In this paper we describe the expansion of the two-wave-plate compensator (TWC) method[44] for full-field retardation measurements by use of a polarization microscope. A brief summary of the TWC technique that was presented in an earlier publication is given in Section 2. Its accuracy is compared theoretically and experimentally with that of the Brace–Köhler and Sénarmont techniques for the measurement of small retardations. The experimental procedure for full-field measurements is then presented and tested with a known retardation (Section 3). The full-field TWC is applied to various optical fibers and compared (Section 4). Its accuracy and sensitivity are assessed by comparison with crossed-polarizer images and the Brace–Köhler technique.

2. Two-Wave-Plate Compensator

The TWC method was presented previously for single-point retardation measurements.[44] This technique consists of placing a birefringent sample at 45° from extinction between crossed polarizers. The sample is followed by a compensator wave plate of known retardation. A null of intensity is found by incremental rotation of the compensator and the analyzer to extinguish the linearly polarized light produced for a specific compensator orientation. In this section we summarize the main results of the TWC technique.

A. Working Principle

A detailed analysis of the successive states of polarization of the light propagating through a system composed of two wave plates between crossed polarizers was presented earlier.[44] The different optical elements of the TWC method are represented in Fig. 1. We used this compensator to derive the condition for linearly polarized output in the TWC method as

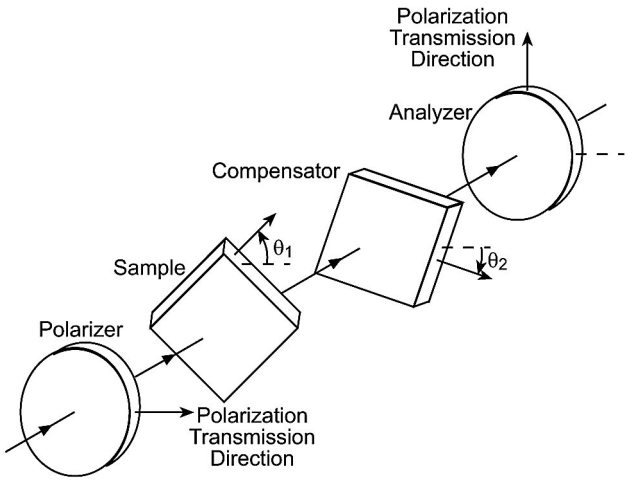

Fig. 1. Two-wave-plate configuration for the TWC method. The sample is 45° from extinction, followed by a compensator wave plate of known retardation. The compensator is rotated to yield a linearly polarized output. We detect a null of intensity by rotating the analyzer.

$$\sin 2\theta_2 = -\frac{\tan \phi_2}{\tan \phi_2}, \tag{1}$$

where ϕ_1 and ϕ_2 are the phase retardations of the two wave plates and θ_2 is the angle between the first polarizer transmission direction and the slow axis of the second wave plate. The first wave plate is oriented at 45° from extinction. In the TWC method, one detects a null of intensity by rotating the analyzer perpendicular to the linearly polarized light produced when the compensator is rotated. Only a brief overview of the performance of the TWC method is given in this section.

B. Accuracy

Computing the intensity transmitted by the two-wave-plate system, we evaluated the measurement error of the TWC technique for single-point retardation measurements for retardations ranging from 0 to λ/8.[44] We calculated the error by considering the measurement uncertainty of the null that is due to the detector's sensitivity. For retardations ranging from 0 to λ/8, 71.41% of the pixels had errors of less than 1%.

In a similar calculation performed for the Brace–Köhler technique, the measurement uncertainty associated with the intensity minimum was considered. Only 22.125% of the pixels had errors of less than 1%. This demonstrates the higher accuracy of the TWC technique for single-point retardation measurements of small retardations.

The TWC technique's accuracy was further evaluated experimentally with a He–Ne laser source and a pair of Glan–Thompson polarizers. Wave plates with small retardations were measured by the TWC, Brace–Köhler, and Sénarmont techniques. Two of the wave plates used were provided with Olympus polarization microscopes. Their retardations were, respec-

Table 1. Comparison of Accuracy of the Two-Wave-Plate Compensator, Brace–Köhler, and Sénarmont Techniques

Crossed Mica Wave Plates	Measured Sample's Retardation (nm)	Technique	Mean Error (nm)	Rank
—	60.33[a]	TWC	0.64	2
		Brace–Köhler	1.24	3
		Sénarmont	0.21	1
—	21.78[a]	TWC	0.24	1
		Brace–Köhler	0.37	2
		Sénarmont	0.46	3
800 nm λ/2, 780 nm λ/2	16.95[b]	TWC	0.58	1
		Brace–Köhler	0.71	2
		Sénarmont	1.11	3
600 nm λ/2, 645 nm λ/2	8.12[b]	TWC	0.30	1
		Brace–Köhler	0.43	2
		Sénarmont	1.88	3
650 nm λ/2, 645 nm λ/2	3.09[b]	TWC	0.97	2
		Brace–Köhler	0.81	1
		Sénarmont	1.07	3
660 nm λ/4, 650 nm λ/4	1.04[b]	TWC	0.19	1
		Brace–Köhler	0.20	2
		Sénarmont	0.50	3

[a]Manufacturer's value.
[b]Difference of two Sénarmont measurements.

tively, 60.33 and 21.78 nm and were specified by the manufacturer to be ±0.01 nm. It is difficult to manufacture accurately zero-order wave plates of retardations less than 10 nm. Therefore, crossed zero-order half-wave plates and quarter-wave plates designed for nearby wavelengths were used to produce small retardations. For example, two mica half-wave plates designed, respectively, for 660 and 645 nm, were measured individually with the Sénarmont technique. Their measured retardations were 328.49 and 320.37 nm. They were then crossed to produce a retardation of 8.12 nm.

The accuracies of the TWC, Brace–Köhler, and Sénarmont techniques can hence be compared. A number of measurements were averaged for each retardation. The average of approximately 20, 40, 60, 20, 30, and 20 measurements was computed for the sample retardations of 60.33, 21.78, 16.95, 8.12, 3.09, and 1.04 nm, respectively. The techniques' accuracies and ranks are summarized in Table 1. The TWC technique achieves the best measurement accuracy for samples with retardations of 1.04, 8.12, 16.95, and 21.78 nm with measurement errors of 0.19, 0.30, 0.58, and 0.24 nm, respectively. The Brace–Köhler technique achieves the best accuracy for only a single sample with a retardation of 3.09 nm with a measurement error of 0.81 nm. The Sénarmont technique also achieves the best accuracy for only a single sample with a retardation of 60.33 nm with a measurement error of 0.21 nm.

3. Full-Field Retardation Measurements

High accuracy and sensitivity of the TWC method have been demonstrated for single-point retardation measurements. Measuring the stress-induced birefringence in optical devices requires, however, much higher spatial resolution. A polarization microscope is used to expand the TWC method from single-point measurements to full-field retardation measurements.

A. Measurement Procedure

The TWC method is implemented for full-field retardation measurements with the polarization microscope system shown in Fig. 2. The microscope used is an Olympus BX-P. The sample is placed on the microscope stage and is observed in transmission between crossed polarizers. The first polarizer is located

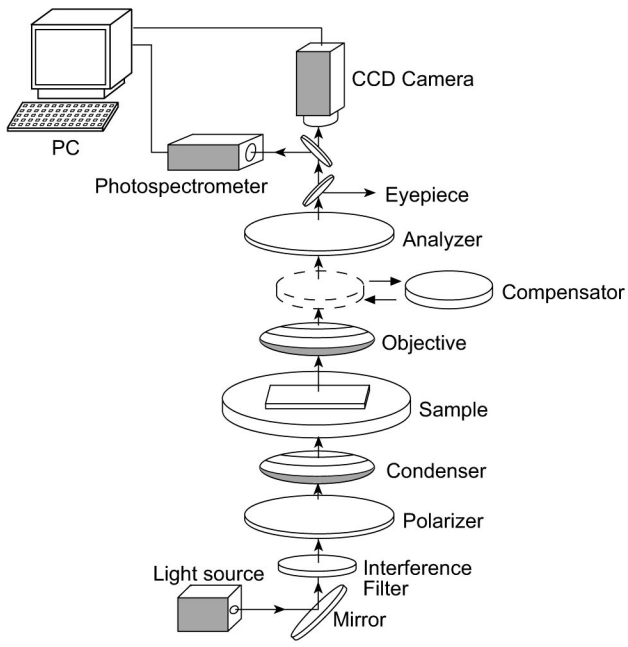

Fig. 2. Polarization microscope system used for full-field retardation measurements.

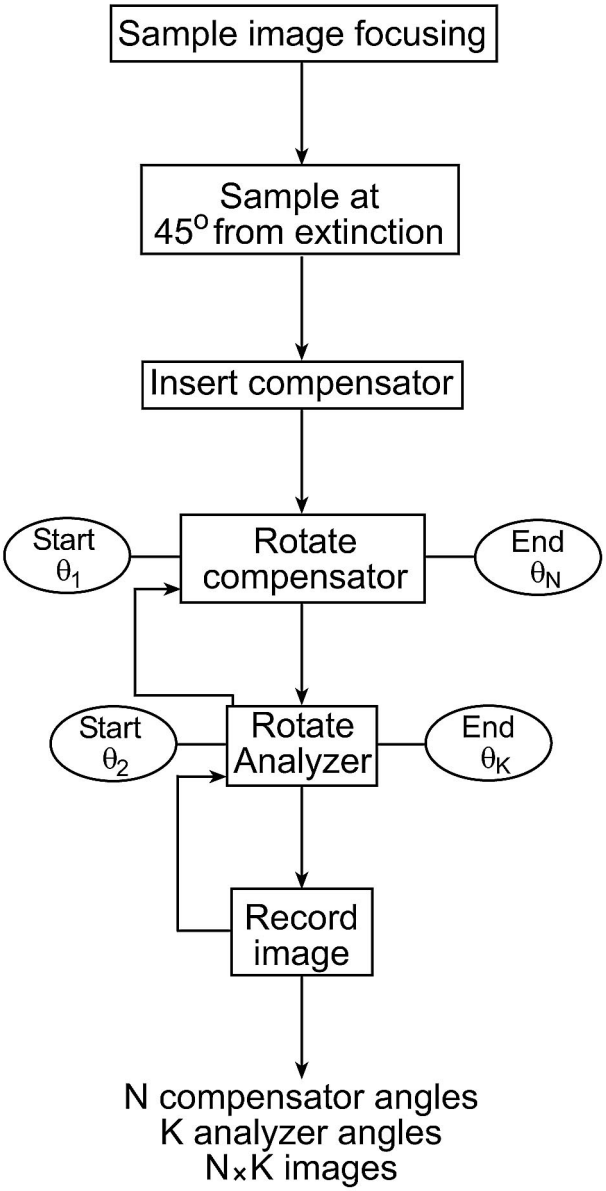

Fig. 3. Flow chart of the image acquisition stage for full-field retardation measurements with the TWC technique.

just before the condenser. The second analyzer is located above the objective. The polarizer and analyzer are rotatable. An insertion slot allows a compensator wave plate to be placed in the microscope tube. The image can be viewed through the eyepiece. A light-path selector knob allows the image to be projected onto a CCD camera connected to a computer. Image processing software allows images to be saved in the computer. The measurements are performed in monochromatic light by insertion of a 546 nm green interference filter with a FWHM of 10 nm in front of the source.

The full-field TWC method consists of two stages: an image acquisition stage and an image processing and analysis stage. The image acquisition stage is represented in a flow chart in Fig. 3. First the sample is focused and oriented at 45° from extinction between crossed polarizers. The compensator is inserted into the microscope tube. Viewing through the eyepiece, we rotate the compensator and the analyzer to estimate the angular ranges for which an extinction is produced for all points over the whole field of view. The compensator's angular range is defined to be θ_1 to θ_N. The analyzer's angular range is defined to be θ_2 to θ_K. Having determined the compensator and analyzer angular ranges, we rotate the compensator from θ_1 to θ_N in small increments, 0.5°, for example. For each successive compensator angle, the analyzer is rotated from θ_2 to θ_K and an image is recorded. Rotating the compensator and the analyzer successively, we record $N \times K$ images corresponding to each successive compensator and analyzer angle. This experimental procedure is performed with and without the sample.

The image processing and analysis stage consists of determining, for each pixel in the field of view (FOV), the analyzer and compensator angles that produce extinction. We determine the extinctions by fitting the variations of the green color component of each pixel (since $\lambda = 546$ nm) to polynomial functions of the compensator and analyzer angles. The minima of those functions are then computed. MATLAB routines are used to process the images and to compute the compensator angle that produces extinction at each pixel within the FOV. We substitute the angular difference between the case with the sample and the case without the sample into Eq. (1) to compute the retardation at each pixel.

Similarly, the Brace–Köhler technique is implemented for full-field retardation measurements. The image acquisition and image processing stages are similar to those for the TWC technique. However, with the Brace–Köhler technique, only the compensator is rotated. An image is recorded at each compensator angle. We then analyze the images to determine at each pixel the compensator angle that produces an intensity minimum. The angular difference between the case with the sample and the case without the sample permits the calculation of the retardation at each pixel.

B. Measurements

Two different compensator wave plates are provided with Olympus microscopes with which we measure retardations by the Brace–Köhler technique. They can be used with green interference filters to measure the retardation of a sample viewed through the eyepiece. The retardations of these two compensators, U-CBR1 and U-CBR2, are specified by the manufacturer and are, respectively, 59.66 and 21.54 nm. The U-CBR2 is placed on the microscope stage, and the U-CBR1 is inserted into the compensator slot of the microscope tube.

We follow the procedure outlined in Subsection 3.A for the TWC technique to record images while the compensator and analyzer are rotated. The sample is then removed from the microscope stage. The compensator is rotated between crossed polarizers, and images are also recorded without the sample. We

process the images recorded with the sample to determine the compensator angle that produces extinction at each pixel. We also process the images recorded without the sample to determine the compensator angles that produce extinction. The angular difference between the two configurations corresponds to θ_2 in Eq. (1). Substituting the measured value of θ_2 and the phase retardation value ϕ_2 of the compensator into Eq. (1) allows the phase retardation ϕ_1 of the sample at each pixel to be calculated. The angles that produce extinction with and without the sample as well as the measured retardation are as shown in Fig. 4(a)–4(c). For this experiment we obtained the images by using an objective magnification of 10×.

The relative error compared with the manufacturer's retardation value was calculated for each pixel. This detailed error analysis shows that 97.9% of the pixels in the FOV were below 4% error and 69% were below 3%. The same sample was also measured with the Brace–Köhler technique. In that case, 99.7% of the pixels in the FOV were below 3% error.

The TWC method appears to be slightly less accurate over the whole FOV than the Brace–Köhler technique. The retardation measured with the TWC in Fig. 4(c) also exhibits a nonuniform distribution along the diagonal of the FOV from the lower left-hand corner to the upper right-hand corner. We determine the compensator angles for extinction with the sample in Fig. 4(a) by rotating the compensator and the analyzer, whereas we determine the compensator angles for extinction without the sample in Fig. 4(b) by rotating only the compensator between crossed polarizers. The latter case does not take into account the nonuniformities arising from rotating the analyzer in the optical system. Consequently, when we subtract both sets of angles to calculate the retardation with the TWC technique, the nonuniformities that are due to the rotation of the optical components do not cancel.

The compensator angles that produce extinction without the sample are hence determined again by rotation of both the compensator and the analyzer. When this is done, the nonuniformities arising from the rotations of the compensator and the analyzer partially cancel when the angles that produce extinction with and without the sample are subtracted.

These compensator angles for extinction without the sample are represented in Fig. 5(a). The corresponding measured retardation in Fig. 5(b) is more nearly uniform than the retardation measured previously as represented in Fig. 4(c). In fact, a detailed analysis of the error distribution in the FOV confirms the improvement from the previous experiment. More particularly, the number of pixels with errors of less than 3% increased from 69% to 94.3%.

The TWC method has proved to be highly accurate for full-field measurements of small retardation. We can further improve the TWC method by optimizing the optics of the microscope, such as the extinction ratio of the polarizers. This is critical to the TWC technique, as the analyzer is rotated along with the compensator when one is searching for the intensity minima. In the current experimental configuration, the intensity transmitted through the polarizers varies sinusoidally as the polarizer and analyzer are rotated in crossed position. These variations reveal that the light incident on the condenser polarizer is

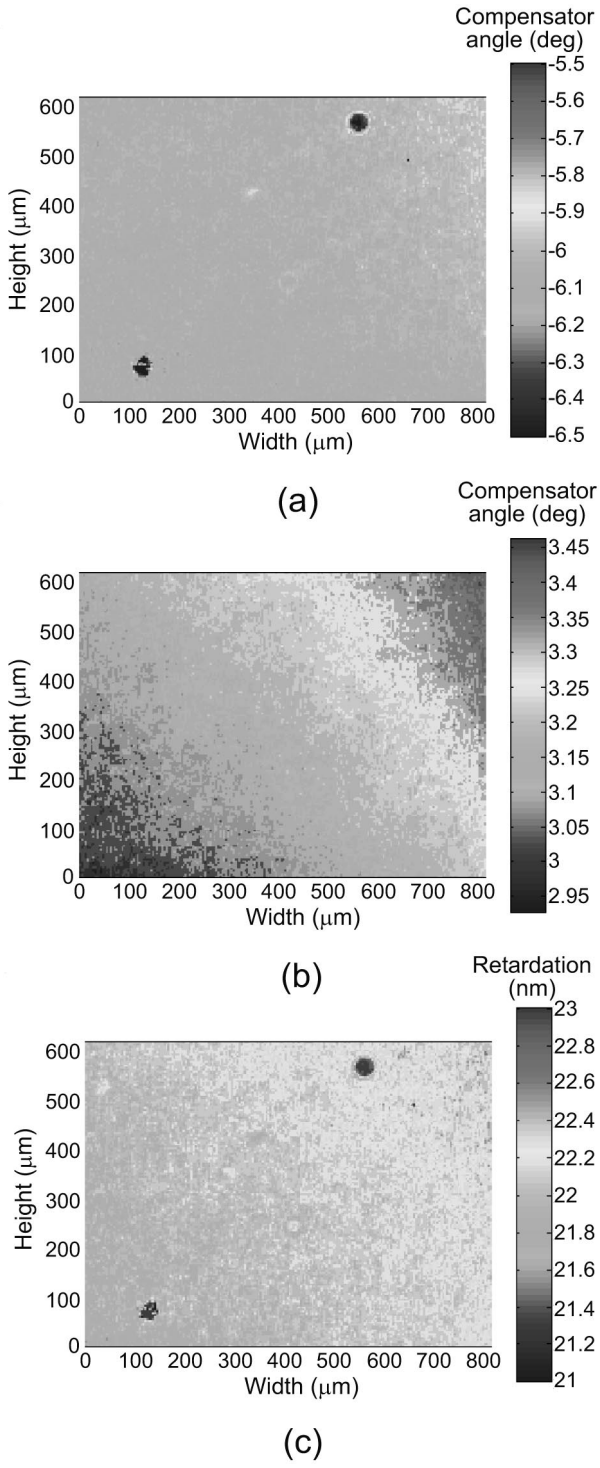

Fig. 4. Full-field retardation measurements with the TWC method. (a) Compensator angles producing extinction with the sample. (b) Compensator angles producing extinction without the sample. (c) Measured retardation.

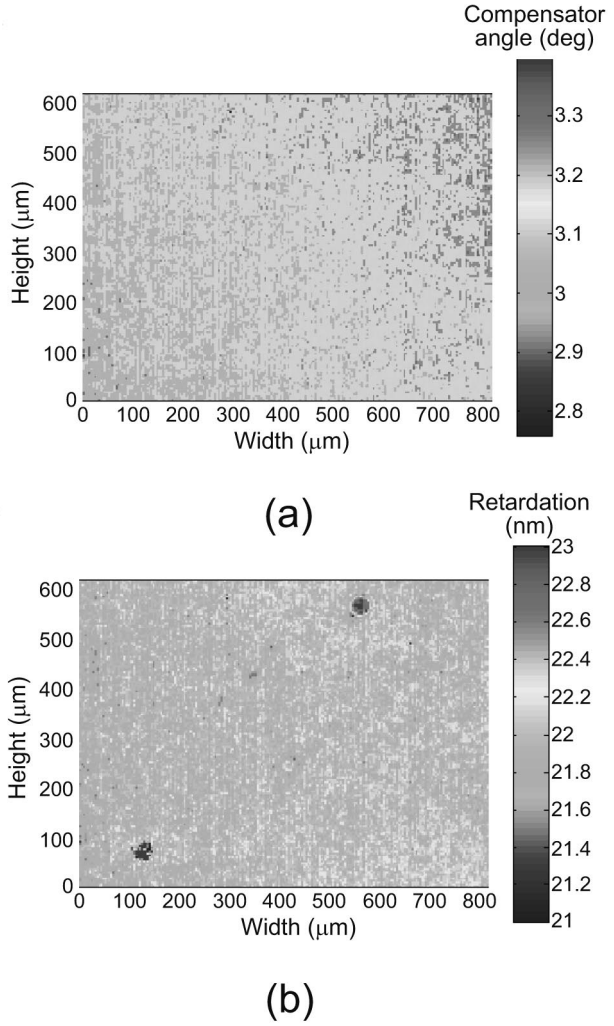

Fig. 5. Full-field retardation measurements with the TWC technique. (a) Compensator angles producing extinction without the sample. (b) Measured retardation.

not randomly polarized. If the light incident on the first polarizer could be made randomly polarized, the extinction would be greatly improved and the TWC's accuracy would be further increased.

4. Application to Optical Fibers

The full-field retardation measurement techniques can be applied to measure the stress-induced birefringence in optical devices. In this section we describe application of the TWC method to map the stress-induced birefringence of different optical fibers by using the experimental procedure presented in Section 3.

A. Polarization-Maintaining Fiber

Polarization-maintaining fibers are used in optical fiber communication networks to preserve the state of polarization of the propagating light. There exist two types of polarization-maintaining fiber, namely, low-birefringence fibers and high-birefringence fibers. In low-birefringence fibers a linearly polarized wave and a circularly polarized wave propagate with

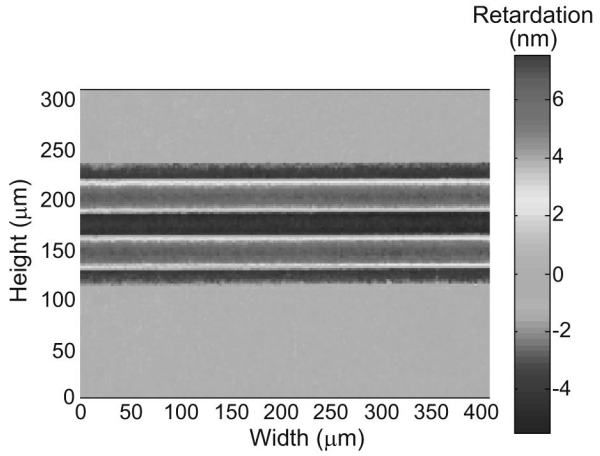

Fig. 6. Polarization-maintaining fiber full-field retardation measurement with the TWC method.

small polarization dispersion. In high-birefringence fibers a linearly polarized wave propagates and remains in its state of polarization.[45]

1. *Full-Field Retardation Measurements*

A polarization-maintaining fiber is placed on a microscope slide made of fused silica whose stress-induced birefringence is negligible compared with that of the fiber. The optical fiber is immersed in index-matching oil and covered by a coverslip that is also made of fused silica.

The retardation of the transversely illuminated polarization-maintaining fiber is measured with the TWC technique. The compensator used is the Olympus Brace–Köhler wave plate U-CBR2 of retardation 21.54 nm at $\lambda = 546$ nm. The resulting two-dimensional retardation distribution is shown in Fig. 6. The objective's magnification is 20×, and its numerical aperture is 0.4, corresponding to a spatial resolution of 0.84 μm. The two high-retardation regions in Fig. 6 correspond to the stress-applying parts.

2. *Comparison with Crossed-Polarizer Images*

The retardation measurements of the high-birefringence polarization-maintaining fiber in Fig. 6 can be used to calculate the transmittance of the light transversely illuminating the fiber to compare with the intensity measured between crossed polarizers and to evaluate the accuracy of the retardation measurements. At such low levels of retardations, a simple crossed-polarizer image results in intensities too weak to be resolved with sufficient dynamic range by the frame grabber. The transmittance comparison is thus made with an image of the optical fiber recorded when the compensator is at an angle, thereby adding a bias retardation and resulting in larger intensities.

The transmittance of a system composed of two wave plates between crossed polarizers had been derived by use of Jones calculus.[44] The reader is encouraged to refer to Ref. 44 about the TWC for single-point retardation measurements for further details

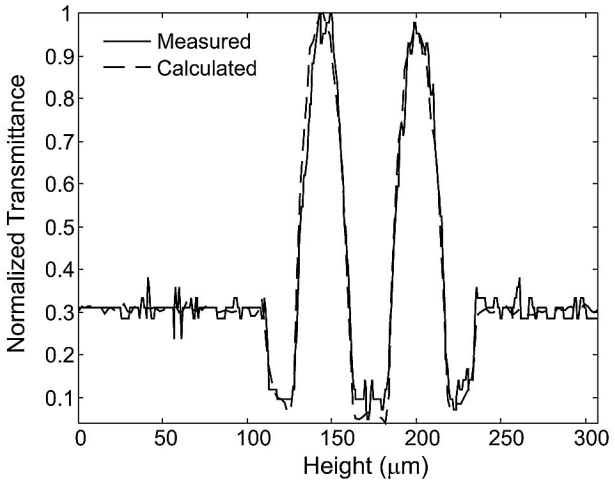

Fig. 7. Comparison of the normalized measured transmittance between crossed polarizers and the normalized transmittance calculated from the retardation of the polarization-maintaining fiber measured by the TWC method shown in Fig. 6.

about the analysis. Knowing the compensator's retardation and orientation, one can use the measured retardation to calculate the transmittance of the transversely illuminated optical fibers, which can thus be compared with the measured transmittances of the crossed-polarizer image.

We used the phase retardation along the fiber cross section in the center of the retardation distribution measured with the TWC technique as shown in Fig. 6 to calculate the transmittance. The image was recorded for a compensator angle equal to 15°. We subtracted the compensator angles for extinction without the sample from this orientation all along the central cross section of the fiber to determine the exact compensator slow-axis orientation. The normalized calculated transmittance is plotted as a dashed curve in Fig. 7. The normalized measured transmittance in the gray-scale image along the same cross section of the optical fiber is plotted as a solid curve in Fig. 7.

The transmittance calculated by use of the retardation profile measured with the TWC method is in good agreement with the measured transmittance shown in Fig. 7. The standard deviation between the measured and calculated transmittances is 0.036. The accuracy of the TWC method for measuring the low-level birefringence in samples such as optical fibers is thus verified.

B. Long-Period Fiber Gratings

Fiber gratings are of great importance in optical fiber communications, as they are used to fabricate band-rejection filters, gain equalizers, and dispersion-compensation devices.[26,27] Long-period fiber gratings (LPFGs), for example, couple the light from a core-guided mode to a cladding-guided mode because of the presence of a periodic refractive-index change along the axis of the optical fiber. In recent years, LPFGs have been fabricated by use of CO_2 laser pulses to modify the refractive-index profile periodically along the axis of an optical fiber.[25–27] These gratings have proved to be more stable than those fabricated by UV exposure. The refractive-index changes induced by the CO_2 laser irradiation are directly related to the amount of residual stress in the optical fiber.[28,29,46] In this section we describe the application of the TWC full-field retardation measurement method to the characterization of LPFGs.

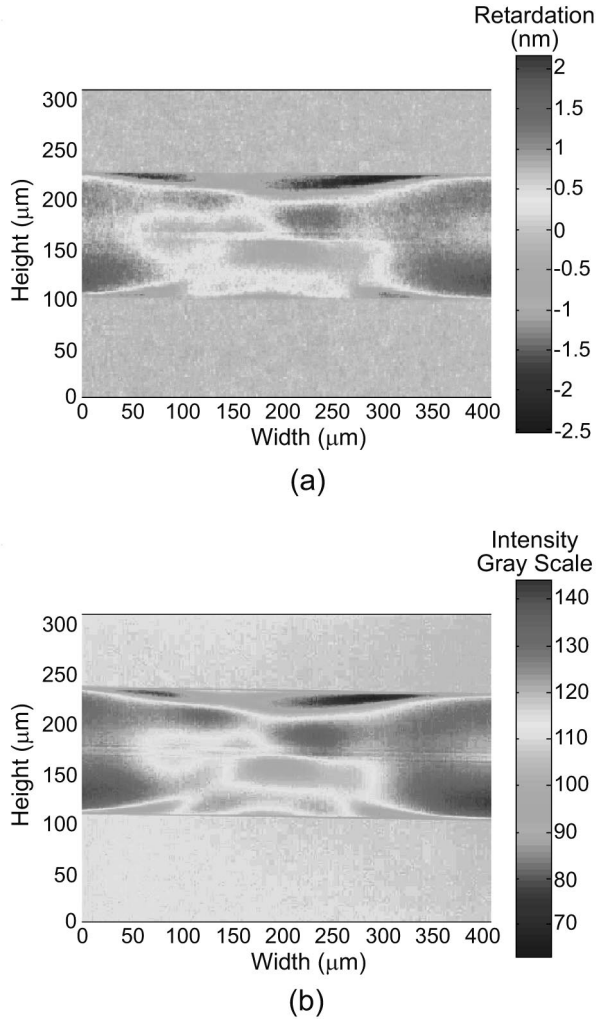

Fig. 8. Comparison of the retardation measurement and the gray-scale image intensity between crossed polarizers of a perturbed region of an overmodulated LPFG. (a) Retardation measurements with the TWC technique. (b) Gray-scale image intensity between crossed polarizers.

1. *Full-Field Retardation Measurements*

The retardation of the perturbed region of a LPFG was measured with the TWC technique and is represented in Fig. 8(a). The grating is overmodulated, exhibiting strong resonances of −15 and −25 dB at wavelengths equal to 1345 and 1440 nm.[26,27]

We can assess the accuracy of the full-field retardation measurement by comparing it with the crossed-polarizer image of the perturbed region of the LPFG in Fig. 8(b). The details of the optical relief revealed in the crossed-polarizer image are quanti-

Table 2. Sensitivity of the Two-Wave-Plate Compensator and Brace–Köhler Techniques

Objective's Magnification	Objective's NA	Brace–Köhler Resolution (nm)	TWC Resolution (nm)
20×	0.40	0.10	0.09
40×	0.75	0.09	0.07

fied on the full-field retardation map. For this measurement the objective magnification was 20× and the objective's numerical aperture was 0.4, which corresponds to a spatial resolution of 0.84 μm. The retardation resolution of the measurement is 0.09 nm, which we evaluated by computing the standard deviation of the background retardation in Fig. 8(a). The TWC full-field retardation measurement is in good agreement with the crossed-polarizer image. The retardation of the unperturbed region of a LPFG, i.e., a region that has not been exposed to the CO_2 laser, can be seen on either side of the perturbed region along the axis of the optical fiber.

The resolution is also calculated in the background of various retardation images generated with the Brace–Köhler and TWC techniques for microscope objectives with magnifications of 20× and 40×. The spatial resolution achieved with the 40× objective is 0.45 μm. The retardation resolutions for the 20× and 40× objectives are summarized in Table 2.

Both the Brace–Köhler and the TWC techniques achieve good resolution. The retardation resolution increases with the objective magnification and numerical aperture. The TWC has a better resolution than the Brace–Köhler technique for the two objective magnifications used. The TWC measurements result in a resolution of 0.07 nm with the 40× objective, whereas the Brace–Köhler measurements result in a resolution of 0.09 nm. The TWC also has better resolution with the 20× objective. These resolutions are very good, especially given the fact that, to find the intensity minima, the compensators are rotated every 0.5°. This angular increment can be decreased to 0.1°, which would further increase the accuracy of the minima determination and reduce the noise floor in the retardation images' background.

2. Comparison with Crossed-Polarizer Images

As with polarization-maintaining fiber, we calculated the transmittance by using the retardation measurements to compare with the measured transmittance of the crossed-polarizer image. The calculated transmittance of the transversely illuminated LPFG is shown in Fig. 9. The calculated transmittance in Fig. 9 is in good agreement with the crossed-polarizer image intensity represented in Fig. 8(b), confirming the high accuracy and high resolution of the full-field TWC method. The details of the birefringence distribution are clearly resolved in the full-field retardation measurements.

This consistency between the measured and calculated transmittances suggests that the retardation

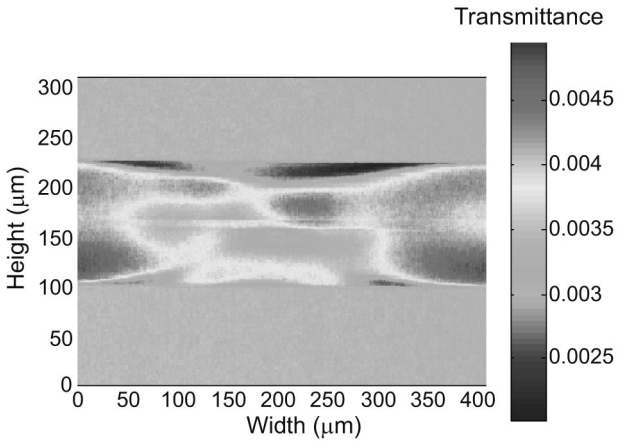

Fig. 9. Transmittance of a transversely illuminated LPFG calculated by use of the retardation measured with the TWC technique shown in Fig. 8(a).

measurements could be used to calibrate the intensity of the crossed-polarizer image. The calibration could be made once with a sample of known retardation. The calibration measurements could then be used with other samples of unknown retardation, obviating the need to use the more lengthy process of the full-field measurements by the TWC techniques. Such a calibration process, however, may be more challenging and less accurate.

Depending on the magnitude of the sample's retardation, different bias retardations are necessary to generate the crossed-polarizer image. Consequently, the calibrations of intensity and retardation would have to be made for different biases corresponding to different retardation magnitudes. Further, the retardation of the unknown sample must be necessarily less than that of the sample used during the calibration, so the measured intensities fall into the calibrated range. This means that the unknown retardation cannot be measured with the calibrated intensities when the sample's retardation is greater than that used for the calibration. The range of retardations that can be measured with the calibrated intensities is therefore limited and constrained to samples whose retardations are less than those used for the calibration.

Most importantly, it is difficult to calibrate the intensities of the retardations because of the nonuniformities that arise from the imperfections in the source or the optical components of the microscope. Residual stress in the objective lenses, for example, affects the formation of the crossed-polarizer image whose intensity depends not only on the birefringence of the sample but also on that of the optical components of the microscope, however small this birefringence might be. This can be better understood if one looks at the retardation measurement of the overmodulated LPFG and the measured transmittance in Fig. 8. The retardation distribution measured with the TWC technique shows a uniform background color in Fig. 8(a) that corresponds to

0 nm retardation. Such is not the case with the intensity of a crossed-polarizer image whose background intensity color varies from the left to the right of the FOV in Fig. 8(b). This nonuniformity is eliminated by a retardation measurement with the TWC technique.

This uniformity can be explained by the fact that the effects that are due to the optical components of the system are canceled with the TWC technique because the retardation measurements are based on subtracting compensator angles that produce extinction with and without the sample. When we subtract the two angles over the whole FOV to compute the retardation, the instrumentation effects are eliminated and only the sample's birefringence is calculated. Thus the TWC technique is more accurate than the intensity measurement technique because of this instrumentation compensation.

5. Conclusions

The two-wave-plate compensator[44] was expanded to full-field retardation measurements. The full-field TWC method used a polarization microscope connected to a CCD camera and a computer to process images and compute the retardation at all pixels. The TWC method was tested on a wave plate of 21.54 nm and achieved an accuracy of 0.06 nm. The spatial resolution achieved was 0.84 μm, and the sensitivity was 0.09 nm with an objective magnification of 20×. Measurements performed with a 40× objective increased the TWC technique's spatial resolution to 0.45 μm and its retardation resolution to 0.07 nm. This resolution is better than that of the Brace–Köhler technique for the same objective, which achieved a resolution of 0.09 nm. The full-field TWC method was applied to the characterization of polarization-maintaining fibers and LPFGs. The TWC retardation measurements were in good agreement with the crossed-polarizer images.

This study was performed as part of the Interconnect Focus Center research program at the Georgia Institute of Technology and was supported by the Microelectronics Advanced Research Corporation and the Defense Advanced Research Projects Agency.

References

1. K. Kitamura, S. Kimura, Y. Miyazawa, Y. Mori, and O. Kamada, "Stress-birefringence associated with facets of rare-earth garnets grown from the melt; a model and measurement of stress-birefringence observed in thin sections," J. Cryst. Growth **62,** 351–359 (1983).
2. K. Kitamura, Y. Miyazawa, Y. Mori, S. Kimura, and M. Higuchi, "Origin of difference in lattice spacings between on- and off-facet regions of rare-earth garnets grown from the melt," J. Cryst. Growth **64,** 207–216 (1983).
3. K. Kitamura, N. Lyi, and S. Kimura, "Growth-induced optical anisotropy of epitaxial garnet films grown on (110)-oriented substrates," J. Appl. Phys. **60,** 1486–1489 (1986).
4. J. M. Desse, "Three-color differential interferometry," Appl. Opt. **36,** 7150–7156 (1997).
5. I. Bloomer and R. Mirsky, "Broadband spectrophotometry: a fast, simple, accurate tool," Photonics Spectra **36,** 86–92 (2002).
6. A. Redner, "Photoelastic measurements by means of computer-assisted spectral-contents analysis," Exp. Mech. **25,** 148–153 (1985).
7. A. Redner, "Photoelastic measurements of residual stresses for NDE," in *Photomechanics and Speckle Metrology*, F.-P. Chiang, ed., Proc. SPIE **814,** 16–19 (1987).
8. R. Oldenbourg, E. D. Salmon, and P. T. Tran, "Birefringence of single and bundled microtubules," Biophys. J. **74,** 645–654 (1998).
9. K. Katoh, K. Hammar, P. Smith, and R. Oldenbourg, "Birefringence imaging directly reveals architectural dynamics of filamentous actin in living growth cones," Mol. Biol. Cell **10,** 197–210 (1999).
10. B. Cense and T. C. Chen, "*In vivo* depth-resolved birefringence measurements of the human retinal nerve fiber layer by polarization-sensitive optical coherence tomography," Opt. Lett. **27,** 1610–1612 (2002).
11. R. Kasahra, M. Itoh, Y. Hida, T. Saida, Y. Inoue, and Y. Hibino, "Birefringence compensated silica-based waveguide with undercladding ridge," Electron. Lett. **38,** 1178–1179 (2002).
12. C. Dragone, "Optimum design of a planar array of tapered waveguides," J. Opt. Soc. Am. A **7,** 2081–2093 (1990).
13. C. Dragone, "An $N \times N$ optical multiplexer using a planar arrangement of two star couplers," IEEE Photon. Technol. Lett. **3,** 812–815 (1991).
14. M. Zirngibl, C. Dragone, and C. H. Joyner, "Demonstration of a 15 × 15 arrayed waveguide multiplexer on InP," IEEE Photon. Technol. Lett. **4,** 1250–1253 (1992).
15. M. Y. Park, S. C. Gwak, K. S. Choi, J. K. Oh, H. J. Lee, and G. H. Song, "Reduction in polarisation-dependent loss and birefringence of arrayed-waveguide grating by adaptable thermal quenching," Electron. Lett. **39,** 54–55 (2003).
16. S. H. Jeong, T. Mizumoto, K. Nakatsuhara, M. Takenaka, and Y. Nakano, "Deep-ridge distributed feedback waveguide for polarisation independent all-optical switching," Electron. Lett. **37,** 498–499 (2001).
17. S. H. Jeong, H. C. Kim, T. Mizumoto, J. Wiedmann, S. Arai, M. Takenaka, and Y. Nakano, "Polarisation insensitive deep-ridge vertical-groove DFB waveguide for all-optical switching," Electron. Lett. **37,** 1387–1389 (2001).
18. G. W. Scherer, "Thermal stress in a cylinder: application to optical waveguide blanks," J. Non-Cryst. Solids **34,** 223–238 (1979).
19. G. W. Scherer, "Stress-induced index profile distortion in optical waveguides," Appl. Opt. **19,** 2000–2006 (1980).
20. G. W. Scherer, "Stress-optical effects in optical waveguides," J. Non-Cryst. Solids **38,** 201–204 (1980).
21. K. Dossou, S. LaRochelle, and M. Fontaine, "Numerical analysis of the contribution of the transverse asymmetry in the photo-induced index change profile to the birefringence of optical fiber," J. Lightwave Technol. **20,** 1463–1469 (2002).
22. P. L. Chu and T. Whitbread, "Measurement of stresses in optical fiber and preform," Appl. Opt. **21,** 4241–4245 (1982).
23. X. Zhao, C. Li, and Y. Z. Xu, "Stress-induced birefringence control in optical planar waveguides," Opt. Lett. **28,** 564–566 (2003).
24. S. Y. Cheng, K. S. Chiang, and H. P. Chan, "Birefringence in benzocyclobutene strip optical waveguides," IEEE Photon. Technol. Lett. **15,** 700–702 (2003).
25. B. L. Bachim and T. K. Gaylord, "Polarization-dependent loss and birefringence in long-period fiber gratings," Appl. Opt. **42,** 6816–6823 (2003).
26. D. D. Davis, T. K. Gaylord, E. N. Glytsis, S. G. Kosinski, S. C. Mettler, and A. M. Vengsarkar, "Long-period fibre grating fabrication with focused CO_2 laser pulses," Electron. Lett. **34,** 302–303 (1998).
27. D. D. Davis, T. K. Gaylord, E. N. Glytsis, and S. C. Mettler,

"Very-high-temperature stable CO_2-laser-induced long-period fibre gratings," Electron. Lett. **35,** 740–742 (1999).
28. B. H. Kim, Y. Park, T. J. Ahan, D. Y. Kim, B. H. Lee, Y. Chung, U. C. Paek, and W. T. Han, "Residual stress relaxation in the core of optical fiber by CO_2 laser irradiation," Opt. Lett. **26,** 1657–1659 (2001).
29. B. H. Kim, T. J. Ahan, D. Y. Kim, B. H. Lee, Y. Chung, U. C. Paek, and W. T. Han, "Effect of CO_2 laser irradiation on the refractive-index change in optical fibers," Appl. Opt. **41,** 3809–3815 (2002).
30. Y. Park, T. J. Ahn, Y. H. Kim, W. T. Han, U. C. Paek, and D. Y. Kim, "Measurement method for profiling the residual stress and the strain-optic coefficient of an optical fiber," Appl. Opt. **41,** 21–26 (2001).
31. T. C. Oakberg, "Measurement of low-level strain birefringence in optical elements using a photoelastic modulator," in *International Symposium on Polarization Analysis and Applications to Device Technology*, T. Yoshizawa and H. Yokota, eds., Proc. SPIE **2873,** 17–20 (1996).
32. B. Wang, "An improved method for measuring low-level linear birefringence in optical materials," in *Inorganic Optical Materials*, A. J. Marker III, ed., Proc. SPIE **3424,** 120–124 (1998).
33. T. C. Oakberg and A. J. Bryan, "Use of detectors with photoelastic modulators," in *Polarization Measurement Analysis and Applications V*, D. H. Goldstein and D. B. Chenault, eds., Proc. SPIE **4819,** 1–8 (2002).
34. B. Wang and T. Oakberg, "A new instrument for measuring both magnitude and angle of low level linear birefringence," Rev. Sci. Instrum. **70,** 3847–3854 (1999).
35. B. Wang, "Accuracy assessment of a linear birefringence measurement system using a Soleil–Babinet compensator," Rev. Sci. Instrum. **72,** 4066–4070 (2001).
36. B. Wang, "Linear birefringence measurement instrument using two photoelastic modulators," Opt. Eng. **41,** 981–987 (2002).
37. B. Wang, J. List, and R. R. Rockwell, "A Stokes polarimeter using two photoelastic modulators," in *Polarization Measurement Analysis and Applications V*, D. H. Goldstein and D. B. Chenault, eds., Proc. SPIE **4819,** 1–8 (2002).
38. R. Oldenbourg and G. Mei, "New polarized light microscope with precision universal compensator," J. Microsc. **180,** 140–147 (1995).
39. M. Schribak and R. Oldenbourg, "Techniques for fast and sensitive measurements of two-dimensional birefringence distributions," Appl. Opt. **42,** 3009–3017 (2002).
40. K. W. Raine, R. Feced, S. E. Kanellopoulos, and V. A. Handerek, "Measurement of axial stress at high spatial resolution in ultraviolet-exposed fibers," Appl. Opt. **38,** 1086–1095 (1999).
41. Y. Park, U. C. Paek, and D. Y. Kim, "Complete determination of the stress tensor of a polarization-maintaining fiber by photoelastic tomography," Opt. Lett. **27,** 1217–1219 (2002).
42. Y. Park, U. C. Paek, and D. Y. Kim, "Determination of stress-induced intrinsic birefringence in a single-mode fiber by measurement of the two-dimensional stress profile," Opt. Lett. **27,** 1291–1293 (2002).
43. Y. Park, U. C. Paek, and D. Y. Kim, "Characterization of a stress-applied polarization-maintaining (PM) fiber through photoelastic tomography," J. Lightwave Technol. **21,** 997–1004 (2003).
44. C. C. Montarou and T. K. Gaylord, "Two-waveplate compensator method for single-point retardation measurements," Appl. Opt. **43,** 6580–6595 (2004).
45. J. Noda, K. Okamoto, and Y. Sasaki, "Polarization-maintaining fibers and their applications," J. Lightwave Technol. **4,** 1071–1089 (1986).
46. C. S. Kim, Y. Han, B. H. Lee, W. T. Han, U. C. Paek, and Y. Chung, "Induction of the refractive index change in B-doped optical fibers through relaxation of the mechanical stress," Opt. Commun. **185,** 337–342 (2000).